CIRCULAR RING E-PLANE ELEMENT PATTERN INTEGRAL REPESENTATION AND ITS ASYMPTOTIC EVALUATION

Aly E Fathy, A. Hessel

The University of Tennessee, ECE Dept., Knoxville, Tennessee 37996

Abstract:

Asymptotic evaluation of the far field for large kr_o results in an analytical expressions, which provides a significant physical insight into the physical process-taking place in element pattern formation.

I- Representation of a Single Element Excitation

Fig. (1) schematically illustrates a circular array of N open ended parallel plate-waveguides, in a perfectly conducting cylinder coated with a dielectric cover. The waveguides are assumed to propagate solely the TEM mode. Only the i = o element is fed, the others are match terminated.

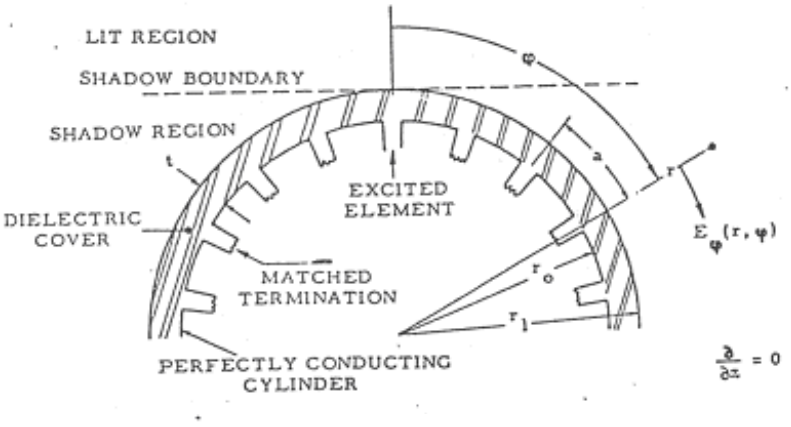

Figure 1 Cross section of a ring array

The integral representation, regards an infinitely extended space $-\infty \le \phi \le \infty$, in which the 2π periodicity is enforced by image elements and periodic image sources, the latter placed an angular distance 2π apart. In this infinite angular space, the actual, physical single element excitation is a superposition of the excitation of individual sources (s=0, ±1,…). Each source is represented in terms of a band spectrum of angular wave numbers ν.

Denoting the angular electric field component by $E_\phi(r,\phi;\nu)$ that would result from such an excitation, i.e. the field due the excitation of the *i*= o element. In the feed waveguide, the modal voltages V_m^i and currents I_m^i are defined in the usual manner. The field at an arbitrary r in the external radial waveguide, can be expressed in terms of the field at r = r_1, as

$$E_\phi(r,\phi,\nu) = \frac{V_{inc}}{\beta r_1}\sqrt{\frac{Y_o^i}{G_a(\nu_o)}}T(\nu,\nu_o)\sum_{m=-\infty}^{m=\infty}\frac{V_m^e(r_1,\nu_m)}{V^i(r_o,\nu_m)}\frac{H_{\nu_m}^{(2)'}(k_o r)}{H_{\nu_m}^{(2)'}(k_o r_1)}e^{-j\nu_m\phi} \qquad (1)$$

where $\nu_m=\nu+2\pi/\beta m$, and $\beta=2\pi/N$. Expression (1) relates the external field resulting from phase sequence excitation, to the incident wave voltage V_{inc}, via the transmission coefficient $T(\nu,\nu_o)$ and the voltage ratio $V^e(r_1,\nu_m)/V^i(r_o,\nu_m)$, both of which are dependent on the form of aperture electric field but not on its on its complex amplitude. Y^i_o is the admittance of the fundamental guide mode, and G_a is the real part of the active

Report Documentation Page

Form Approved
OMB No. 0704-0188

1. REPORT DATE	2. REPORT TYPE	3. DATES COVERED
23 APR 2004	**N/A**	**-**

4. TITLE AND SUBTITLE	5a. CONTRACT NUMBER
Circular Ring E-Plane Element Pattern Integral Repesentation And Its Asymptotic Evaluation	5b. GRANT NUMBER
	5c. PROGRAM ELEMENT NUMBER
6. AUTHOR(S)	5d. PROJECT NUMBER
	5e. TASK NUMBER
	5f. WORK UNIT NUMBER
7. PERFORMING ORGANIZATION NAME(S) AND ADDRESS(ES) **The University of Tennessee, ECE Dept., Knoxville, Tennessee 37996**	8. PERFORMING ORGANIZATION REPORT NUMBER
9. SPONSORING/MONITORING AGENCY NAME(S) AND ADDRESS(ES)	10. SPONSOR/MONITOR'S ACRONYM(S)
	11. SPONSOR/MONITOR'S REPORT NUMBER(S)

12. DISTRIBUTION/AVAILABILITY STATEMENT
Approved for public release, distribution unlimited

13. SUPPLEMENTARY NOTES
See also ADM001763, Annual Review of Progress in Applied Computational Electromagnetics (20th) Held in Syracuse, NY on 19-23 April 2004.

14. ABSTRACT

15. SUBJECT TERMS

16. SECURITY CLASSIFICATION OF:			17. LIMITATION OF ABSTRACT	18. NUMBER OF PAGES	19a. NAME OF RESPONSIBLE PERSON
a. REPORT	b. ABSTRACT	c. THIS PAGE			
unclassified	**unclassified**	**unclassified**	**UU**	**12**	

Standard Form 298 (Rev. 8-98)
Prescribed by ANSI Std Z39-18

admittance Y_a.

II- Element Pattern

Expressions for the field resulting from a single element excitation are obtained with the help of (1), and the use of $2\pi/\beta$ periodicity in the ν of the Floquet fields, where $T(\nu,\nu_o)=T(\nu_m,\nu_o)$, and in view of the identity $\int_{-\frac{\pi}{\beta}}^{\frac{\pi}{\beta}}\sum_{m=-\infty}^{\infty} f(\nu+\frac{2\pi}{\beta}m)d\nu=\int_{-\infty}^{\infty} f(\nu)d\nu$, the infinite sum of the finite integrals in (1) may be replaced by a single infinite integral [1,2,3], i.e.

$$E_\phi^o(r,\phi)=\frac{V_{inc}}{2\pi r_1}\sqrt{\frac{Y_o^i}{G_a(\nu_o)}}\int_{-\infty}^{\infty} T(\nu,\nu_o)\frac{V^e(r_1,\nu)}{V^i(r_o,\nu)}\frac{H_\nu^{(2)'}(k_o r)}{H_\nu^{(2)'}(k_o r_1)}e^{-j\nu\phi}d\nu \qquad (2)$$

As $k_o r\to\infty$, even though $\nu<\infty$, it is permissible in (2) to use directly the large argument, first order asymptotic expression for the derivative of $H^{(2)'}(k_o r)$. Therefore, the far field corresponding to (2) becomes

$$E_\phi^o=-jV_{inc}/2\pi r_1\sqrt{Y_o^i/G_a(\nu_o)}\sqrt{2/\pi k_o r}\,e^{-j(k_o r-\frac{\pi}{4})}\int_{-\infty}^{\infty} T(\nu,\nu_o)V^e(r_1,\nu)/V^i(r_o,\nu)\frac{e^{-j\nu(\phi-\frac{\pi}{2})}}{H_\nu^{(2)'}(k_o r_1)}d\nu \qquad (3)$$

III- Transmission Coefficient T(ν, ν_o)

III-1 Active Admittance:

When the form of the aperture field is a slowly varying function of ν, the behavior of the transmission coefficient determines the element pattern and hence, is of a very special importance. Where the transmission coefficient is function of the active reflection coefficient $\Gamma_a(\nu)$ given by:

$$T(\nu,\nu_o)=1+\Gamma_a(\nu,\nu_o),\qquad \Gamma_a(\nu,\nu_o)=(Y_a(\nu_o)-Y_a(\nu))/(Y_a^*(\nu_o)+Y_a(\nu)) \qquad (4)$$

From (4) it is seen that the active admittance $Y_a(\nu)$ uniquely specifies $T(\nu,\nu_o)$ for a given match point ν_o. An approximate expression for $Y_a(\nu)$ can be obtained as in planar arrays from the requirement of continuity of complex power at the aperture in a unit cell [1,2]:

$$Y_a(\nu)=I_o^i(r_o,\nu)/V_o^i(r_o,\nu)=\sum_{m=-\infty}^{\infty}\left|V^e(r_o,\nu_m)\right|^2/\left|V_o^i(r_o,\nu)\right|^2 Y^e(r_o,\nu_m)+\sum_{p=1}^{\infty}\left|V_p^i(r_o,\nu)\right|^2/\left|V_o^i(r_o,\nu)\right|^2 Y_p^i \qquad (5)$$

where Y^e and Y^i are respectively the modal admittance of the radial and TEM guides. Since and the voltage ratios in (5) depend on the form of the aperture electric field, $\underline{E}_{ap}$, $Y_a(\nu)$ may be calculated only provided this form is known. For the case of a single mode aperture mode will be treated as an example. The first term in the right hand side of (5) represents the contribution of the exterior region to the input admittance and is strongly ν-dependent because of the form of the dominant radial mode characteristic admittance $Y^e(r,\nu)$ at $r=r_o$ which is is given by [3]

$$Y^e(r_o,\nu)=G^e(r_o,\nu)+jB^e(r_o,\nu)=\frac{1}{\varsigma_o\beta r_o}Y^{e'}(r,\nu)=\frac{-j}{\varsigma_o\beta r_o}\frac{H_\nu^{(2)}(kr_o)}{H_\nu^{(2)'}(kr_o)}=\sqrt{\varepsilon_r}\,\frac{1+\Gamma\frac{H_\nu^{(1)}(kr_o)}{H_\nu^{(2)}(kr_o)}}{1+\Gamma\frac{H_\nu^{(1)'}(kr_o)}{H_\nu^{(2)'}(kr_o)}} \qquad (6)$$

where, $k = k_o\sqrt{\varepsilon_r}$ and the air-dielectric interface reflection coefficient Γ is

$$\Gamma = \frac{H_\nu^{(2)'}(k_o r_1)}{H_\nu^{(1)'}(k_o r_1)} \frac{\sqrt{\varepsilon_r} Y_\nu'(kr_1) - Y_\nu'(k_o r_1)}{\sqrt{\varepsilon_r}\, \bar{Y}_\nu(kr_1) + Y_\nu'(k_o r_1)}, \text{ and } Y_\nu'(kx) = -j\frac{H_\nu^{(2)}(kx)}{H_\nu^{(2)'}(kx)}, \qquad \bar{Y}_\nu = j\frac{\bar{H}_\nu^{(1)}(kx)}{H_\nu^{(1)'}(kx)} \quad (7)$$

III-2 Zeros of T (ν, ν_o) and Surface Wave Resonance of an Unperforated Cylindrical Structure:

$T(\nu,\nu_o)$ exhibits zeros at the poles of $Y_a(\nu)$. These occur at the value of ν for which $Y^e(r_o, \nu_m) = \infty$. These surface wave roots for imperfect structure occur for complex values of ν [1,2]. By continuity argument with the planar case, this type of resonance is expected to occur for a value of Real(ν) for which the air region is "cut-off" and the dielectric propagating. In such case, $kr_1 > \mathrm{Re}(\nu) > k_o r_1$. As was pointed out, these poles do not lie on the real ν-axis, as in the planar case, since an attenuated, angularly propagating surface wave is not possible in the cylindrical case.

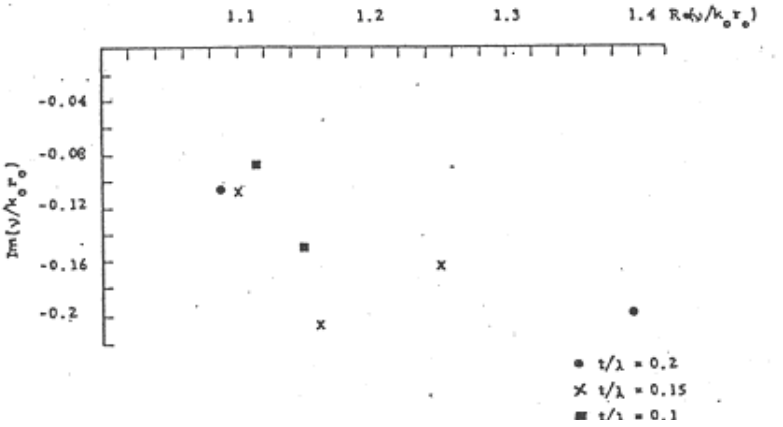

Figure 2 Root Locations as function sheet thickness

It manifests itself in a resonant behavior of the imaginary part of $Y_a(\nu)$, where the latter experiences a sharp rise and a sign reversal (but does not become infinite like in the planar case) in the predicted range for a value of $\mathrm{Re}(\nu/k_o r_1)$, almost equal to that for the corresponding planar case. The location of this resonance depends on the dielectric sleeve thickness. It is seen that if (t/λ) is small the resonance moves into transition region where ($\nu = k_o r_1$). While thicker dielectric covers, locate this surface wave in a region where Debye's approximation is valid for the different cylindrical functions. The modal admittance reduces to:

$$Y^{e'} = \frac{\sqrt{\varepsilon_r}}{\cos w_{kr_o}} \frac{\sqrt{\varepsilon_r}\cos w_{k\,r_1} - \chi\cos w_{kr_1}}{\sqrt{\varepsilon_r}\cos w_{k_o r_1} + \chi\cos w_{kr_1}} \quad (8)$$

where $\chi = -j\cot(\varsigma_{kr_1} - \varsigma_{kr_o})$ and

$$\xi_{kr} = kr(\cos w_{kr} - (\frac{\pi}{2} - w_{kr})\sin w_{kr}), \sin w_{kr} = \nu/kr \quad (9)$$

Hence, in the Debye region the dispersion relation (8, 9) for the surface wave on smooth conducting cylinder covered with a dielectric sleeve reduces to

$$\sqrt{\varepsilon_r}\cos w_{k_o r_1}\chi - \cos w_{kr_1} = 0 \quad (10)$$

Fig. 2 shows typical root location of (10) vs. sleeve thickness in the complex ν-plane. In the limit $k_o r_o \to \infty$ reduces to relations previously derived in the planar case, i.e. to the lowest TM surface wave on a grounded dielectric slab as was pointed out earlier.

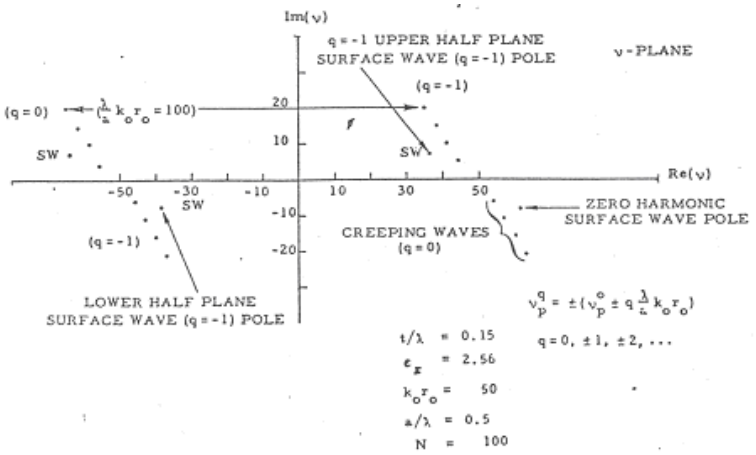

Figure 3 Pole Singularities of T(ν)

III-3 Poles of T(ν,ν$_o$):

From (4), the poles of T(ν,ν$_o$) (see Fig. 3) are the natural resonance of the match-terminated array structure, and correspond to the periodic solutions of the transverse resonance equation where

$$Y_a^*(\nu_o) + Y_a(\nu_m^p) = 0,\ \nu_m^p = \nu_o^p + m2\pi/\beta, (m = 0,\pm1,\ldots), (p = 0,\pm1,\ldots) \quad (11).$$

The pole location of the match terminated cylindrical array structure is a perturbation on that of the short-circuited structure. The dispersion relation of the later corresponds to the poles of the m = 0 term in Y$_a$(ν), i.e. ν_o^p. Equation (11) has two relevant sets of significant poles. One arises by perturbation due to finite curvature of the planar TM guided waves on a planar match terminated array structure. The other, the familiar creeping waves which are a perturbation of those on a full dielectric cylinder, by bringing the perforated conducting cylindrical surface into proximity of the air-dielectric interface. The location of the latter is near ν = k$_o$r$_1$.

In the planar case, the wave numbers of the corresponding transverse resonance equation were found to correspond to leaky waves and the fundamental slow harmonic wave number was found to be near the surface wave number of the short-circuited array structure shows various pole locations for different dielectric thickness. In the cylindrical case, a similar situation exists for the first set of significant poles where, for the set m = 0 of (12) the relevant surface wave pole is in a region of validity of Debye approximation. In this case, to first order, the modal admittances are identical to the corresponding planar expression. Since, the creeping waves pole locations are in the transition region, i.e. of $H_\nu^{(2)}(k_o r_1)$, ν=k$_o$r$_1$ and different modal admittance representation must be used

$$Y^{e'} = \frac{\sqrt{\varepsilon_r}}{\cos w_{kr_o}} \frac{\frac{\sqrt{\varepsilon_r}}{\cos w_{kr_1}} Ai'(\tau)Z + je^{j\frac{2\pi}{3}}(\frac{k_o r_1}{2})^{1/3} Ai(\tau)}{\frac{\sqrt{\varepsilon_r}}{\cos w_{kr_1}} Ai'(\tau) + je^{j\frac{2\pi}{3}}(\frac{k_o r_1}{2})^{1/3} ZAi(\tau)} \quad (12)$$

where $\nu = k_o r_1 + (\frac{k_o r_1}{2})^{1/3} \tau e^{j\frac{2\pi}{3}}$, $\sin w_{kr} = \frac{\nu}{kr_1}$, $Z = \frac{1 - e^{-j2(\varsigma_{kr_1} - \varsigma_{kr_o})}}{1 + e^{-j2(\varsigma_{kr_1} - \varsigma_{kr_o})}} = j\tan(\varsigma_{kr_1} - \varsigma_{kr_o})$

where Ai is Airy function and ζ_{kr} is given by

$\varsigma_{kr} = kr(\cos w_{kr} - w_{kr}(\pi - w_{kr})\sin w_{kr})$.

IV- Asymptotic Evaluation of Far Fields

The integral representation may be evaluated asymptotically for large values of kr_1 yielding simple analytical expressions. The asymptotic evaluation of (3) proceeds in a manner similar to smooth large cylinder or uncovered cylindrical array [1].

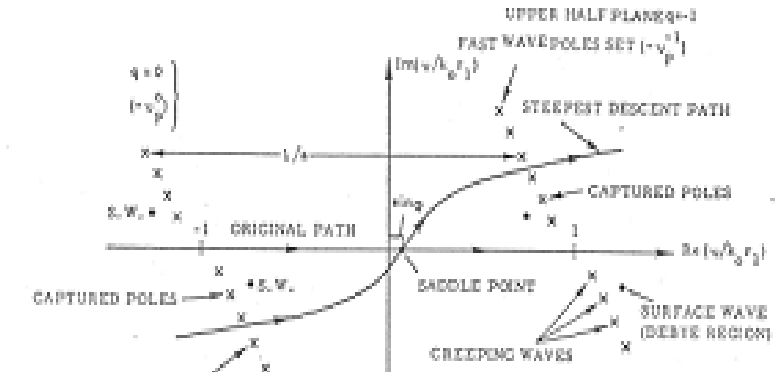

Figure 4 Contour deformation in the lit region

Different representations are obtained for the lit region, the shadow region and the shadow boundary (see Fig. 1). By virtue of the Physical space $-\pi \le \varphi \le \pi$, is in the shadow region of the image sources $s \neq 0$. This shadow region is in general considerably deeper than that for s=0 source and consequently the contribution from $s \neq o$ are neglected except near $\varphi = \pm\pi$; (details follow later). Hence, the lit region and the shadow boundary transition region are pertinent only to the s =0 source.

A. Lit Region

The basic integral in (12) to be evaluated is of the form

$$F(\phi) = \int_{-\infty}^{\infty} T(\nu, \nu_o) V^e(r_1, \nu) / V^i(r_o, \nu) e^{-j\nu(\phi - \frac{\pi}{2})} / H_\nu^{(2)'}(k_o r_1) d\nu \qquad (13)$$

under the assumptions that the saddle point of this integrand lies in region where Debye approximation [1] of $H_\nu^{(2)'}$ can be used (this assumption will be justified later), i.e. $|\nu_s - k_o r_1| > O(k_o r_1)^{1/3}$ hence, the integral (13) becomes

$$F(\phi) = \sqrt{\frac{\pi k_o r_1}{2}} e^{j\frac{\pi}{4}} \int_{-\infty}^{\infty} T(\nu, \nu_o) \frac{V^e(r_1, \nu)}{V^i(r_o, \nu)} \frac{e^{-jk_o r_1 \psi(\nu)}}{\sqrt{\cos w_{k_o r_1}}} d\nu \qquad (14)$$

where $\sin w_{k_o r_1} = \nu / kr_1$ and $\psi(\nu) = (\phi - w)\sin w - \cos w$

For a given value of ϕ, the saddle point ν_s or w_s are located at $d\psi / d\nu = o$, i.e. at

$$\phi = w_s \qquad or \sin\phi = \sin w_s = \nu_s / k_o r_1 \qquad (15)$$

Since the range of w_s is limited to $-\pi/2 < w < \pi/2$ therefore, has a $d\psi / d\nu = o$. This

condition assures that $\nu_s < k_o r_1$, and justifies the assumption of validity of Debye approximation for $H_\nu^{(2)}(k_o r_1)$. This solution is valid only in the lit region. Thus the steepest-descent path (S.D.P) through the saddle point is defined by:

$$\mathrm{Re}\,\psi(\nu) = \mathrm{Re}\,\psi(\nu_s) = -\cos\phi \tag{16}$$

The deformability of the original contour into the S.D.P. in the ν-plane may be ascertained by investigation of the behavior of the integrand as $|\nu| \to \infty$. By Cauchy's theorem one has (see Fig. **4**)

$$\int_{-\infty}^{\infty} \{\}\, d\nu = \int_{S.D.P.} \{\}\, d\nu + 2\pi j \sum_{p,q} [\mathrm{Re}\, s(-\nu_p^q) - \mathrm{Re}\, s(\nu_p^q)] \tag{17}$$

In contrast to smooth cylindrical structures, the appearance of pole contributions in the lit region is due to the angular periodicity of the array. The evaluation of the integral in the lit region is complicated by the fact that the transmission coefficient may have poles near or on the S.D.P. **(Fig. 4).** In the development to follow, the first order saddle point contribution, the pole residues, and the transition pattern function due to the presence of a pole near the saddle point are obtained.

1: First Order Saddle Point Contribution

Upon substitution of

$$F(\Omega) = \int f(x) e^{j\Omega q(x)} dx = \sqrt{2\pi / \Omega \left| q''(x) \right|} f(x_s) e^{j\Omega q(x_s)} e^{\pm j\frac{\pi}{4}}$$
$$\Omega \to \infty \qquad for \qquad q''(x) \gtrless 0 \tag{18}$$

the first order S.D.P contribution (direct ray) to (13) becomes

$$E^o_{\phi(S.D.P.)}(r,\phi) = k\frac{V_o^{inc}}{2}\sqrt{\frac{Y_o^i}{G_a(\nu_o)}}\frac{V^e(r_1, k_o r_1 \sin\phi)}{V^i(r_o, k_o r_1 \sin\phi)} T(k_o r_1 \sin\phi)\sqrt{\frac{2}{\pi k_o r}} e^{-j(k_o r - \pi/4 - k_o r_1 \cos\phi)} \tag{19}$$

This contribution is observed solely in the lit region, appears to originate from the center of the cylinder and is referred as the "direct contribution" or "the space wave".

2. Pole Contributions: From (41), the residue at a typical fast wave pole of ν_p^q of T(ν)

$$\mathrm{Re}\, s(\nu_p^q) = e^{j\frac{\pi}{4}} V^e(r_1, \nu_p^q) / V^i(r_o, \nu_p^q) \sqrt{\pi k_o r_1 / 2\cos w_{\nu_p^q}}\, a_p e^{-jk_o r_1 \psi(\nu_p^q)} \tag{20}$$

while the Residue a_p is given by $a_p = \lim_{\nu \to \nu_p^q} (\nu - \nu_p^q) T(\nu)$ (21)

In (20), the pattern ϕ dependence enters exclusively through the exponential; the remainder of the expression depends only on the pole location and represents the excitation coefficient for surface waves or creeping waves. The poles of T(ν) are $\pm\nu_p^q$ and for q= 0 represent the harmonics of the fundamental q = 0 set. With the help of (26) and (47), a typical fast wave pole contribution to the radiated electric field becomes

$$E_\phi^0(r,\phi)|_{pole} = -j\sqrt{Y_o^i / G_a(\nu_o)} V^e(r_1, \nu_p^q) / V^i(r_o, \nu_p^q) \sqrt{\pi k_o / 2 r_o \cos w_{\nu_p^q}}\, a_p e^{-j(k_o r + k_o r_1 \psi(\nu_p^q))} \tag{22}$$

As seen from Fig. **9**, only the q <0 poles are captured in the lit region. For element

spacing ½<a/λ<1, the poles corresponding to q < -1 (2) lie in the region |Re(ν/k$_o$r$_1$)|>1 where exponentially increasing with |ν|. Hence, the dominant pole contributions in the lit region [1,2] are those corresponding to q = -1, for which |Re(ν/k$_o$r$_1$)|<1, and for w_i is small. The exponent in (49) is found to be

$$-jk_o r_1 \psi(-\nu_p^{-1}) = -j(\phi - |w_r|)|\nu_r| + + jk_o r_1 \cos w_r + |\nu_i|(\phi - |w_r|) + j\frac{\pi}{4} \qquad (23)$$

where $\nu = \nu_r + j\nu_r$, $\quad w = w_r + jw_i$ and for $(-\nu_p^{-1}), \nu_r > 0, \nu_i > 0, w_r > 0, w_i > 0)$.

A similar phase expression for those poles located at ν= ν_p^{-1} and is given by

$$-jk_o r_1 \psi(\nu_p^{-1}) = j(\phi + |w_r|)|\nu_r| + jk_o r_1 \cos w_r - |\nu_i|(\phi + |w_r|) + j\frac{\pi}{4} \qquad (24)$$

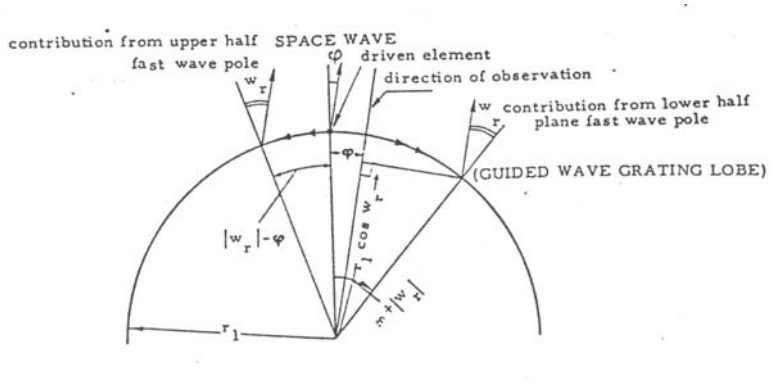

Figure 5 Ray Contributions in the lit Region

where ν_r <o,ν_i,<o, w_r <o,w_i <o for ν_p^{-1} poles. The first term (23) expresses the fact that with increasing ϕ, for ϕ>0 the effect of this set is more pronounced (undergoes less attenuation), and has maximum contribution when the S.D.P. crosses

a relevant pole, i.e., ($\phi = w_r$ (which is the pole transition region). On the other hand, (24) shows that, this set has less effect, more attenuation, as ϕ is increased for ϕ>o. For the case of lower half plane poles (w_i<*o, w_r <o,* ν_i.<o, ν_r<o) the real part of (24) indicates that a typical ray travels clockwise through an angle (ϕ + |w_r|)| along the surface and decays at a rate of |ν_i |> nepers/radians. The first term in the imaginary part of (24) represents the phase change as the phase change as the ray travels from the source along the surface; its associated phase velocity is sin (w_r)<0, and the ray thus represents a backward fast wave. The second term in the imaginary part of (24) is the phase referenced to the cylinder center, associated with the free space path of the ray and implies that, irrespectively of ϕ, the fast set emerges from the surface at a constant angle w_r with the local normal (the positive angles are clockwise), as shown in Fig. **5**.

Rays due to upper half plane poles follow a path which is the mirror image of that for the lower half plane poles, and (23), (19) show that, this set of poles has a phase difference with that of the direct ray given by $\Delta\phi \approx k_o r_1(\cos\phi - \cos w_r) + \nu_r / k_o r_1(\phi - w_r)$, where w_r *>o,*w_i>o and very small, ν_r>o. Fast Wave Pole Transition When the integral along the steepest descent path is approximated by the saddle point contribution, this overall result experiences a discontinuity as a function of ϕ every time the path crosses a pole, the discontinuity being proportional to the pole residue. For poles deep in the complex plane, this residue is exponentially small and the transition effect may be neglected. For poles close to the real axis, their proximity to the S.D.P. may be taken into account and a

continuous transition field. The overall result of the asymptotic evaluation of the integral (13) is given by the sum of the saddle point contribution (19), the residue contribution from the fully captured poles (22) and the contribution from the transition poles. The latter harmonic q = -1 set, passes through this transition, where S.D.P. crosses the surface wave root ($-\nu_o^{-1}$) first, then ($-\nu_p^{-1}$) for p> 0 and the contribution is given by

$$F(\phi)|_{transition\_pole} = e^{j(k_o r_1 \cos\phi + \frac{\pi}{4})} \sum_p V^e(\nu_p^q) / V^i(\nu_p^q) a_p \sqrt{\pi k_o r_1 2\cos w_p^q}\, \chi_p \qquad (25)$$

$$\sin w_p^{-1} = \frac{-\nu_p}{k_o r_1}; q = -1 \quad and \quad \chi_p = 1/b_p\sqrt{\pi/k_o r_1} + j2\pi e^{-jk_o r_1 b_p^2} Q(-jb_p\sqrt{k_o r_1/\sqrt{\pi}}$$

Q(y) is the transition function given by the complementary error function

$$Q(y) = \int_{-\infty}^{\infty} e^{-x^2} dx \quad , \text{and } b_p = e^{j\pi/4}\sqrt{\psi(\nu_p^{-1}) + \cos\varphi} \qquad (26)$$

B. Shadow Region $\pi/2 < |\phi| < \pi$

The integral ($\pi/2<\phi<\pi$) can be expressed as a residue series at the poles of T(ν). For element spacing ½<a/λ<1, the contributions in the shadow region come mainly from the sources s = 0, and s= ±1. The contributions of all other sources are highly attenuated, as they have to travel long angular distances to reach the physical space $-\pi<\phi<\pi$. For example, for $F(\varphi) = 2\pi j \sum_{p,q} \mathrm{Re}\, s(\nu_p^q) + 2\pi j \sum_{p,q} \mathrm{Re}\, s(-\nu_p^q)$. Where for s=0, the path of integration is closed at the lower half-plane, and for s = 1, it is closed at the upper half plane, as shown in Fig. **6**. A clear picture is captured by studying the phase for the slow wave sets = 0, q = 0, where:

$$-jk_o r_1 \psi(\nu_p^0) \approx -|\nu_i|(\varphi + |w_r| - \pi) - jk_o r_1(\cos w_r + |\nu_r|/k_o r_1.(\varphi - \pi + |w_r|) - j\pi/4 \qquad (27)$$

but, $w_r \approx \pi/2$ and $w_r<0$, $\nu_r<0$. So for those slow waves in the lower half-plane one has $\nu_i<0$, $\nu_r>o$, Consequently $-jk_o r_1\psi(\nu_p^0) \approx -|\nu_i|(\varphi - \pi/2) - j\nu_r(\varphi - \pi/2) - j\pi/4$ The first term of (27) gives an attenuation as if it were traveling an angular distance $(\varphi + |w_r| - \pi \approx \varphi - \pi/2)$ with an attenuation factor $|\nu_i|$. A corresponding relation is found in the phase, i.e, the second term in (27), which shows a forward wave travels a positive angle $(\varphi + |w_r| - \pi \approx \varphi - \pi/2)$ from the excited element with a positive phase velocity, as shown in **Fig. 11b**, while the third term ($jk_o r_1 \cos w_r \approx 0$), so when the phase is combined with ($-jk_o r$), indicates that the wave departs from the surface at a point **B** (to which it travels on the surface an angular distance ≈ $\phi - \pi/2$ and radiates to the observation point at the angle ($\pi - |w_r| \approx \pi/2$) with respect to local normal). For fixed p, the higher terms of the higher harmonics, i.e., q>0 are exponentially decreasing as, $\nu > k_o r_1$ and the Hankel function derivative blows up, as well as ($-|w_i|\ |\nu_r| + k_o r_1 \sin|w_r| \sinh|w_i| < 0$) and gives more attenuation with increasing ν_r and fixed $|\nu_i|$ as $\nu_r > k_o r_1$. For the set q= -1, the total complex phase is rewritten as

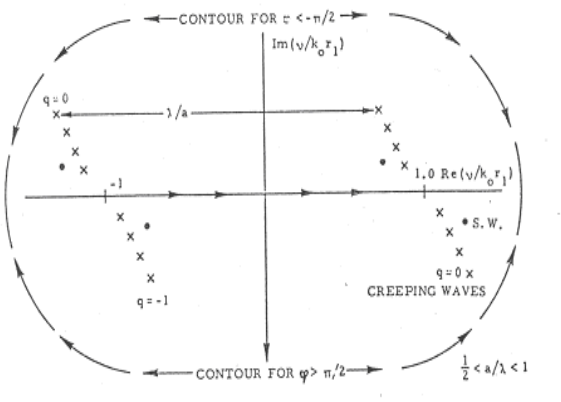

Figure 6 Contour deformation for shadow region

$$-jk_o\psi(\nu_p^{-1}) \approx -|\nu_i|(\varphi+|w_r|)+j(|\nu_r|+(\varphi+|w_r|+k_o r_1\cos w_r) \tag{28}$$

the first term shows that the wave attenuates as it moves an angular distance (ϕ+|w_r|) with an attenuation factor |ν_i|. It is clear that this term is greater than the angle traveled by the same p wave but for the set, q=o, and consequently corresponds to higher attenuation for this term and hence q=o is the dominant term for the source s=o (see Fig. **7**).

To account for the contributions of the source s=1 ($\pi/2<\phi<\pi$), the contour must be closed in the upper half plane as shown in Fig. **7**, it **is** required to replace ϕ by (ϕ -2π), hence the total phase is given by

$$-jk_o r_1\psi(-\nu_p^0) \approx |\nu_i|(\varphi-|w_r|-\pi)-jk_o r_1\cos w_r + j|\nu_r|(\varphi-\pi-|w_r|) \tag{29}$$

where the first term of (29) shows that as if the wave traveling the angular distance |ϕ–π-|w_r|| with an attenuation rate |ν_i|. This angular distance is larger than that of the set (q=o, s=o), i.e., more attenuation is experienced, but it is only comparable to it if $\phi \approx \pi$, which will interfere with it giving ripples in the element pattern gain near $\phi \approx \pi$. While the second term of (29) shows that this wave has negative phase velocity with negative angle, so it is a forward wave.

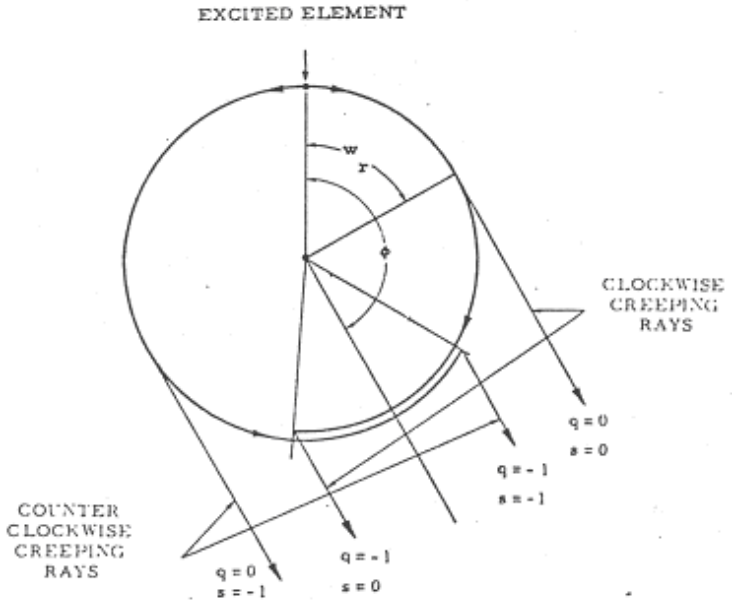

Fig. 7 Ray interpretation in the shadow

Similar considerations for the set s =1, q = -1, with the contour of integration is closed in the upper half plane shows that a total phase given by

$$-jk_o\psi(-\nu_p^{-1}) \approx |\nu_i|(\varphi-2\pi-|w_r|)-j|\nu_r|(\varphi-2\pi-|w_r|)+jk_o r_1\cos w_r \tag{30}$$

which shows, for the same p, the largest attenuation, due to the longest angle of travel compared to the three other sets, i.e., (s=o, q=0), (s=o, q= -1), (s=1, q=o). It is to be noted that the set of creeping wave poles corresponding to q = o requires special consideration since the Airy approximation must be used for the Hankel functions in the vicinity of $\nu \approx k_o r_1$. In general, the residue

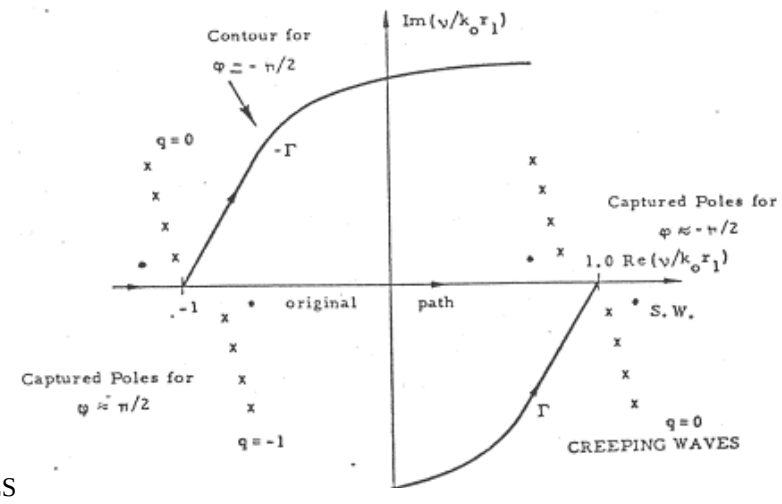

Figure 8 Contour in the shadow boundary

at ν_p^o corresponding to a creeping wave:

$$\text{Res}|_{(\nu_p^o)_{creeping}} = V^e(\nu_p^o)/V^i(\nu_p^o)e^{-j\nu_p^o(\varphi-\pi/2)}/H_{\nu_p}^{(2)'}(k_o r_1)a_p, \tag{31}$$

where a_p is given by (21) given before, For $(\phi-\pi/2)>0$ (sufficiently large), the residue series is rapidly convergent, since contribution from successive values of p decay exponentially. However, when $(\varphi-\pi/2)\le(k_o r_1)^{-2/3}$ i.e. in the shadow boundary, the convergence slows down and an alternate technique must be used.

C. Shadow Boundary

Near the shadow boundary the harmonic series is poorly convergent, and the techniques used in the lit region cannot be extended since the Debye approximation to the Hankel functions is not valid for $\nu \approx k_o r_1$. This difficulty has already been resolved for smooth cylinders with surface admittance [1]. We can ascertain that the integrand decays exponentially away from $\nu/k_o r_1 = 1$ along the path Γ. Thus, the integral along Γ in may be approximated, and from the large argument approximation for the Airy function [1] we can ascertain that the integrand decays exponentially away from $\nu/k_o r_1 \approx /1$ along the path Γ (see Fig. 8). Thus the integral along Γ in may be approximated by

$$F(\varphi)|_\Gamma = -(k_o r_1)V^i(k_o r_1, r_o)/V^e(k_o r_1, r_1)2G_a(\nu_o)k\sqrt{\varepsilon_r r_1/r_o}\,e^{-j(\varsigma_{kr_1}-\varsigma_{kr_o})} \tag{32}$$

where $k = e^{-jk_o r_1(\varphi-\pi/2)}g((k_o r_1)^{1/3}(\varphi-\pi/2);\alpha)$

and $g(\varsigma,\alpha) = \int_{\infty e^{-j2\pi/3}}^{\infty} e^{-j\varsigma\tau}/(Ai(2^{1/3}\tau e^{-j2\pi/3}) + \alpha Ai(2^{1/3}\tau e^{-j2\pi/3}))d\tau$ (33)

The shadow boundary transition function $g(\varsigma,\alpha)$ is a generalization of the Fock function.

V. Example:

Single Mode Aperture Field Approximation

For illustration purposes, a TEM parallel plate waveguide-fed array is considered. The aperture field is assumed to be uniform across the aperture. Matching the array under the equi-phase condition $\nu = 0$ (broad-side scan), was selected for all calculations. The numerical evaluation of the E-plane element patterns was performed with the help of harmonic series for a number of dielectric sleeve thickness with $\varepsilon_r = 2.56$, $k_o r_o = 50$ and $a/\lambda = 0.5$. Figs. **(9),(10)** show main features of the E-plane element voltage gainpatterns, normalized to the unit cell gain $\sqrt{2\pi a/\lambda}$.

The presence of a dielectric cover on the cylindrical array is seen to introduce a pronounced dip, and pattern ripple near broadside, which tend to be larger than those of uncovered circular arrays with $a/\lambda >$o. The location of the pattern dip is essentially identical to that observed in corresponding planar arrays with a dielectric cover of the same thickness. It is observed that radomes of increased thickness, the dip moves towards broadside and becomes more pronounced. More ripples between broadside and the dip are observed for thinner covers, while in the shadow region almost a constant slope (on a dB scale) is found. Characterization of these features is obtained by the asymptotic valuation of the Integral representation. The results of this calculation are plotted in Figs. (**9**) and (**10**) for different radome thickness with $k_o r_o = 50$.

In the lit region $0<\phi<90°$, the total pattern is the result of the superposition of the space

wave (saddle point contributions) and contributions from fast wave poles. These poles were considered in pairs ($\pm\nu_p^{-1}$). In numerical evaluation, their number was varied to include just a surface wave contribution p=o, or in addition up to four creeping waves (p = 0, 1, 2, 3, 4), the ripple in the main beam in the lit region is found due to the interference between the space wave and the fast set of poles ($\pm\nu_p^{-1}$). However, it was determined that, only the surface wave pole ($\pm\nu_0^{-1}$) contribution has a significant effect in the lit region. An approximate prediction of the location of the dip can be made by the planar formula $\sin\varphi = \left|\nu_o^o / k_o r_1 - \lambda / a\right|$, where ν_o^o / r_1 is the surface wave number. The location of the planar array nulls is indicated by arrows in Figs. (**9**), and (**10**). The pattern in the shadow region was computed by the residue series via only the slow wave poles (ν_p^o for $\phi > 90^o$), where p was varied from o to 3.

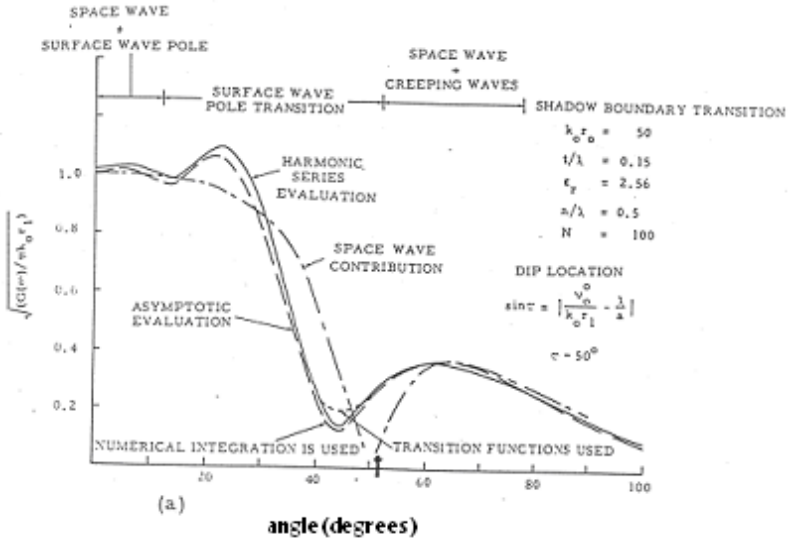

Figure 9 Element Gain Pattern.

Deep in the shadow region, the pattern is due to the wave with the lowest attenuation constant, which in the examples given is the first slow creeping wave (p = 1, q = 0, s = 0). For $\phi = \pi$, interference between the two lowest creeping waves (s=+1, p=1, q=0) and (s =0, p =1, q =0) for yields the well-known back-lobe ripple of the pattern. A detailed break down of the various wave contributions to the element pattern is discussed in Fig. (**9**). It is seen that the dip in the space wave appears near 44.6^o. For $0<\phi<15°$ and $50°<\phi<75°$, the influence from the captured fast creeping wave poles and the surface waves ($(\nu_o^{-1}, -\nu_o^{-1})$ as considered as their respective residue contributions. In the region $15^o << \phi < 50^o$, the pole transition effects were taken into account.

As seen from Fig. **9** the general outline of the pattern in the lit forward region is determined by the space wave. By comparing the results of harmonic series with that of superposition of the space wave and surface wave residue contribution, one concludes as mentioned that, the ripple in the main beam may be directly attributed to interference between the space wave and the fast surface wave pole. In addition, to obtain a good accuracy, one clockwise and one counterclockwise fast creeping wave should be taken into account. Again, the pattern in the shadow region (see Figs. **9, 10**) was computed sing residue series of only slow wave poles (ν_p^o for $\pi/2<\phi<\pi$), whose number was also

varied from p= o to 3. This produced sufficient accuracy obtained even close to the penumbra.

Deep in the shadow region, the slope (in dB) of the element pattern is essentially that of the single lowest creeping wave pole contribution. The pattern in the shadow boundary transition 75° $<\phi<$110° was determined by a numerical integration of the transition function. Fig. **9** shows the element pattern for $k_o r_o$ =50, element spacing a/λ=0.5 ε_r=2.56 and dielectric thickness t/λ=0.2, since dip appears now at an angle =38º and the pattern is correspondingly narrower than for t/λ=0.15. The dip level however, is more pronounced than for t/λ =0.15. Also, the ripple frequency has increased as the wave gets slower. Main factors in the location of the dip is the element spacing a/λ, and the surface wave location, as example, the dip will appear more closer to broadside for larger a/λ as shown in Fig. (**10**) for a dielectric sleeve of t/λ=0.15 with a/λ=0.525. In this case, the dip occurs at an angle 38°, compared to 44.6° shown before for t/λ=0.15 but a/λ=0.5.

For a cylinder of larger radius, the above-mentioned effects are modified. For the case of $k_o r_o$ =105 and a/λ=0.525, the element pattern in the lit region, is dominated by the space wave, while ripple amplitude decreases and its frequency increases as for the case of cylindrical arrays without dielectric radome [1,2].

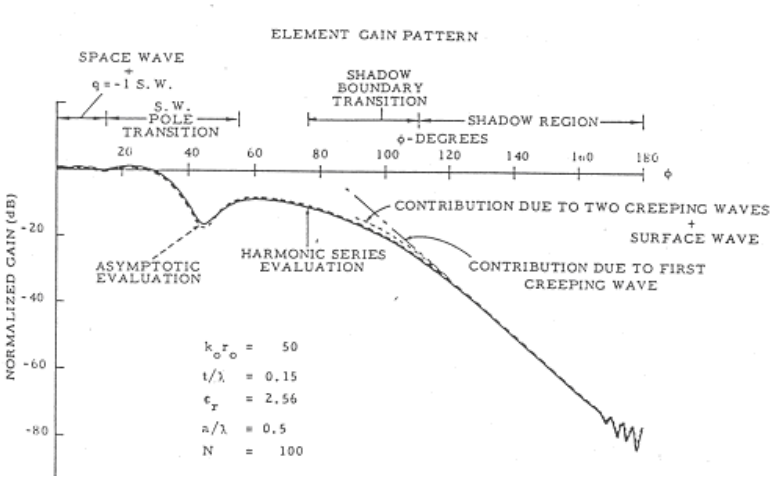

Fig. 10 Element Gain Pattern.

VI-Conclusions:

Guided wave effects are profoundly influenced by curvature, and are clearly displayed in the element pattern in mutually coupled array. Element pattern serves as a sensitive indicator of the degree of suitability of the phased array radome combination. A dielectric sheet in contact with the radiating structure of the phased array gives rise to scan volume limited by blind spots arising when phase synchronization of one of the Floquet modes with guided surface wave-- due to the dielectric cover.

VII-Acknowledgement:

In memory of Prof. Alex. Hessel: A great Man- A Great Educator- and A great Scientist.

VIII- References:

1) J.C. Sureau, Ph.D. thesis, Polytech. Inst. New York, June 1971.

2) A. Hessel and J. C. Sureau," Resonance in circular arrays with dielectric sheet covers, IEEE Trans. Antennas Propagat., Vol. AP-21, pp.159-164, Mar. 1973.

3) A. E. Fathy, Ph.D. thesis, Polytech. Inst. New York, June 1984.

